Bone mineral density measurement in the Gruen zones using dual-energy x-ray absorptiometry

insights from quantitative CT analysis

From Osaka University, Suita, Japan

Cite this article:
Bone Joint Res 2025;14(10):
850–859.

DOI: 10.1302/2046-3758.
1410.BJR-2025-0036.R1

Correspondence should be sent to Keisuke Uemura
surmountjp@gmail.com

K. Uemura,[1] Y. Otake,[2] K. Tamura,[3] R. Higuchi,[4] S. Kono,[4] H. Mae,[4] K. Takashima,[4] S. Okada,[4] N. Sugano,[1] H. Hamada[1]

[1]Department of Orthopaedic Medical Engineering, Osaka University Graduate School of Medicine, Suita, Japan
[2]Division of Information Science, Graduate School of Science and Technology, Nara Institute of Science and Technology, Ikoma, Japan
[3]Department of Orthopaedics, Kyowakai Hospital, Suita, Japan
[4]Department of Orthopaedic Surgery, Osaka University Graduate School of Medicine, Suita, Japan

Aims

After total hip arthroplasty (THA), dual-energy x-ray absorptiometry (DXA) is used as necessary to assess the bone mineral density (BMD) in the Gruen zones around the femoral stem implants. Although periprosthetic BMD may serve as a potential indicator for evaluating stress adaptive remodelling and stem fixation, several factors can introduce measurement errors. Therefore, an automated method was applied using quantitative CT, verified for the total hip with correlation coefficient > 0.9, for BMD assessment in the Gruen zones.

Methods

This was a retrospective analysis of 71 hips from 58 participants (9 male and 49 female) who underwent THA using the same taper-wedge type stem. Preoperative and postoperative CT scans were acquired alongside DXA measurements of the Gruen zones. A deep-learning method was used to measure BMD in the Gruen zones from preoperative CT images by embedding the stem position information acquired from postoperative CT images through iterative closest point registration. CT images were rotated to the neutral position and were projected anteroposteriorly to generate a digitally reconstructed radiograph to measure the BMD at each zone (CT-aBMD). Correlations between CT-aBMD and DXA measurements were assessed for each zone.

Results

The correlations between CT-aBMD and DXA measurements for zones 1 to 7 were 0.924, 0.783, 0.817, 0.921, 0.731, 0.847, and 0.677, respectively ($p < 0.001$ for all).

Conclusion

Our results based on CT analysis suggest that DXA is generally reliable for assessing BMD in the Gruen zones. However, caution may be advised for zones 5 and 7 because of limited correlations. As zone 7 plays a crucial role in stem fixation, during longitudinal evaluation of post-THA stress adaptive remodelling, we recommend ensuring cautious interpretation and consistent BMD measurements using the image attached to the DXA report. It is imperative to calculate the least significant change for accurate BMD evaluation.

Bone & Joint Research

Article focus

- Uses preoperative quantitative CT (qCT) images and computer-aided design (CAD) models, and develops a method to quantify precise bone mineral density (BMD) measurements in the Gruen zones.
- Compares BMD measurements obtained from qCT and dual-energy x-ray absorptiometry (DXA) in all Gruen zones.

Key messages

- Strong to very strong correlations were observed between DXA and qCT measurements for all Gruen zones; however, the correlation was limited to 0.677 in zone 7.
- Special attention is required when interpreting DXA measurements in zone 7, a critical region for evaluating implant fixation and stress transfer.

Strengths and limitations

- Combines qCT and CAD modelling to produce accurate BMD measurements.
- Offers a comprehensive analysis of DXA measurement errors and emphasizes careful interpretation in clinical settings, especially for zone 7.
- Findings are specific to the Accolade II stem, limiting their applicability to other implant designs.

Introduction

Dual-energy x-ray absorptiometry (DXA) is commonly used to measure bone mineral density (BMD) of the lumbar spine and/or the proximal femur to diagnose osteoporosis and initiate treatment for preventing fragile fractures.[1,2] Although mainly used for the lumbar and proximal femur, DXA can measure BMD in other regions such as the radius,[3] knee,[4] and humerus.[5] However, caution is necessary for BMD assessment while using DXA at each region because several factors may induce measurement errors.[6,7] For example, the effect of insufficient setting of the regions of interest (ROIs) and patient positioning on BMD measurement errors is well documented.[8-11]

In total hip arthroplasty (THA), BMD measurement around the femoral stem implant has been considered a potential indicator for assessing stress adaptive remodelling and stem fixation. BMD around the stem is typically classified using Gruen zones.[12] Several studies have reported BMD changes using this classification,[13-19] and performed clinical assessments by analyzing the relationships of BMD in the Gruen zones with the stem insertion angle,[19] stem types,[13,14,20] and osteoporosis medication.[21] Although its measurement precision has been evaluated through repeated analyses, the accuracy of the DXA measurements in the Gruen zones has not been well characterized.[17,18,22,23] In particular, careful exclusion of the implant region is necessary when defining the ROI for each zone because this process is prone to error and the ROI is small. In addition, the effect of hip rotation, shown to have a substantial influence on the BMD measurements of the proximal femur,[8-10] would potentially affect the BMD measurements at the Gruen zone.

Therefore, developing a novel and automatic method for measuring the BMD at the Gruen zones unaffected by the image acquisition or measurement method (e.g. patient positioning and ROI setting), and comparing the results with those measured from DXA, are urgent tasks. To these ends, we aimed to use quantitative CT images (qCT) that provide more detailed information on BMD and are listed on the adult official positions of the International Society for Clinical Densitometry (ISCD) for measuring the BMD of the proximal femur.[24] The purposes of this study were to incorporate postoperative CT images using the implant's computer-aided design (CAD) model and computer simulation to establish a method to measure the BMD at the Gruen zones from preoperative qCT, and to compare BMD measurements and evaluate their differences between DXA and qCT.

Methods

Participants

This retrospective study was approved by the Institutional Review Board and complied with the principles enshrined in the Declaration of Helsinki.[25] Informed consent was obtained in the form of opt-out. A consecutive series of 73 hips of 60 participants who underwent THA between July 2022 and August 2023 using an Accolade II stem with a caput-collum-diaphyseal angle of 127° (Stryker, USA) was initially included in this study. This stem was selected as it was the most frequently used cementless stem during the study period, and is one of the most frequently used stems globally.[26,27] Of the 73 hips, one hip was excluded because of the lack of DXA examination, and one hip was excluded because of a previous hip fracture. Finally, 71 hips of 58 participants (9 male and 49 female) were included for analysis, including 13 participants who underwent bilateral THA (Table I). The mean age, height, weight, and BMI of the participants were 68.0 years (SD 10.1), 154.6 cm (SD 6.8), 58.4 kg (SD 10.4), and 24.3 kg/m^2 (SD 3.6), respectively. The main indication for performing THA was osteoarthritis (69 hips), and the mean preoperative Japanese Orthopaedic Association hip score (min, 0; max, 100) was 54.7 (SD 17.4) (Table I).[28]

CT and DXA acquisition

For all 58 participants, preoperative and postoperative CT scans were acquired using an OptimaCT660 scanner (GE Healthcare Japan, Japan), and DXA was acquired using PRODIGY (GE Healthcare) to measure the BMD at the Gruen zones. CT images were acquired from the pelvis to the knee under the same protocol (tube voltage: 120 kVP; tube current: 115.4 ± 20.9 mA; table height: 148.4 ± 11.0 mm; pixel size: (0.703 to 0.879 mm) × (0.703 to 0.879 mm); matrix: 512 × 512). Slice thickness was 1.25 mm for preoperative CT images and between 1.25 (pelvis to proximal femur) and 10 mm (midfemur) for postoperative CT images. The images were reconstructed with a filtered back projection, and GE Healthcare's standard kernel was applied. Pre- and postoperative CT images were interpolated to an interval of 1 mm. During pre- and postoperative CT image acquisition, a calibration phantom made of urethane foam and containing four hydroxyapatite rods (B-MAS200; Kyoto Kagaku, Japan) was included in the images to convert radiodensity (in Hounsfield units) into bone density (in mg/cm^3). For DXA, a standard calibration recommended by the manufacturer was performed daily, and images were acquired with a leg positioner used to set the patella upward. The definition of the ROI was performed semiautomatically by a trained radiological technologist. The mean duration between preoperative

Table I. Patient demographic data.

Patient demographics	Value
Sex, n (male/female)	9/49
Mean age, yrs (SD)	68.0 (10.1)
Mean height, cm (SD)	154.6 (6.8)
Mean weight, kg (SD)	58.4 (10.4)
Mean BMI, kg/m^2 (SD)	24.3 (3.6)
Hip disease (no. hips)	
OA	69
Osteonecrosis	1
Rapidly destructive coxarthrosis	1
Mean JOA hip score (SD)	54.7 (17.4)
Osteoporosis medication, no. cases	10
Surgical side, n	Left (30), Right (41)
Surgical approach (no. hips)	
Modified Watson-Jones	19
Posterolateral	52
Cup size, mm (no. hips)	
44	1
46	17
48	7
50	26
52	9
54	6
56	2
58	2
62	1
Stem size (no. hips)*	
#1	1
#2	4
#3	17
#4	18
#5	14
#6	12
#7	4
#9	1

*There were no hips with a #8 stem size.
JOA, Japanese Orthopaedic Association.

and postoperative CT was 5.4 weeks (SD 1.0), and the mean duration between preoperative CT and DXA acquisition was 5.5 weeks (SD 0.9).

Image processing

To measure the BMD at the Gruen zone from CT images, we applied a previously validated deep-learning-based method to measure the BMD of the proximal femur (i.e. total region of the hip) which showed a strong correlation with DXA measurements (correlation coefficient: 0.94).[29] As the effect of metal artifacts cannot be entirely avoided when measuring BMD from postoperative CT images, we used CAD models of the stem embedded in preoperative qCT.

First, from postoperative CT images, the femur and the stem were automatically segmented using a previously validated deep-learning model (Figure 1).[30,31] Then, the surface model of the stem region was registered to the CAD model to precisely delineate the position of the stem in the postoperative CT coordinates using iterative closest point (ICP) registration.[32] Next, using the preoperative CT images, the femur and the calibration phantom were automatically segmented, and the landmarks of the femur (tip of the lesser trochanter, centre of the femoral canal 2 and 5 cm distal from the tip of the lesser trochanter, and medial and lateral posterior condyles) were detected using a previously trained and validated deep-learning model.[29,33] Then, the surface model of the femur region proximal to the lesser trochanter was registered to that generated from the postoperative CT images using ICP registration to calculate the femur position in the postoperative CT coordinates. The transformations between the postoperative CT coordinates and the femur and the stem coordinates were concatenated to provide the stem position relative to the femur. Using the transformation, the stem CAD model was embedded in preoperative qCT images (defined as 'CAD-embedded preoperative qCT') to reproduce the stem position in preoperative CT images. This can be considered an artifact-free postoperative CT. The CT images with the CAD model were rotated to the neutral position using the two landmarks (centre of the femoral canal 2 and 5 cm distal from the tip of the lesser trochanter) to compensate for abduction/adduction and flexion/extension. Further, two landmarks (medial and lateral posterior condyles) were used to compensate for internal/external rotation that existed during the acquisition of preoperative CT images. Finally, the rotated CAD-embedded preoperative qCT were projected anteroposteriorly to generate a digitally reconstructed radiograph (DRR), and were classified into Gruen zones 1 to 7 using the length of the stem after excluding the region proximal to the neck-stem junction (Figure 1). Zone 4 was defined as the region within 2 cm from the distal end of the stem, as defined by the DXA manufacturer. From the DRR of each zone, the bone mineral content (CT-BMC), Area (CT-Area), and areal BMD (CT-aBMD, calculated as CT-BMC/CT-Area) were measured (Figure 1). These processes were performed automatically, and the scripts used are available at https://github.com/keisuke-uemura/Gruen-zone-BMD.

Comparison between CT and DXA measurements

CT-BMC, CT-Area, and CT-aBMD measured at each zone were compared to those measured with DXA (i.e. DXA-BMC, DXA-Area, and DXA-BMD). Further, the agreement between the CT-aBMD and DXA-BMD for each region was assessed using the Bland-Altman analysis, and their ranges of limits of agreement (LoA) were also calculated.

Validation

To validate the measurement process applied in this study, the surface distance between the stem region segmented

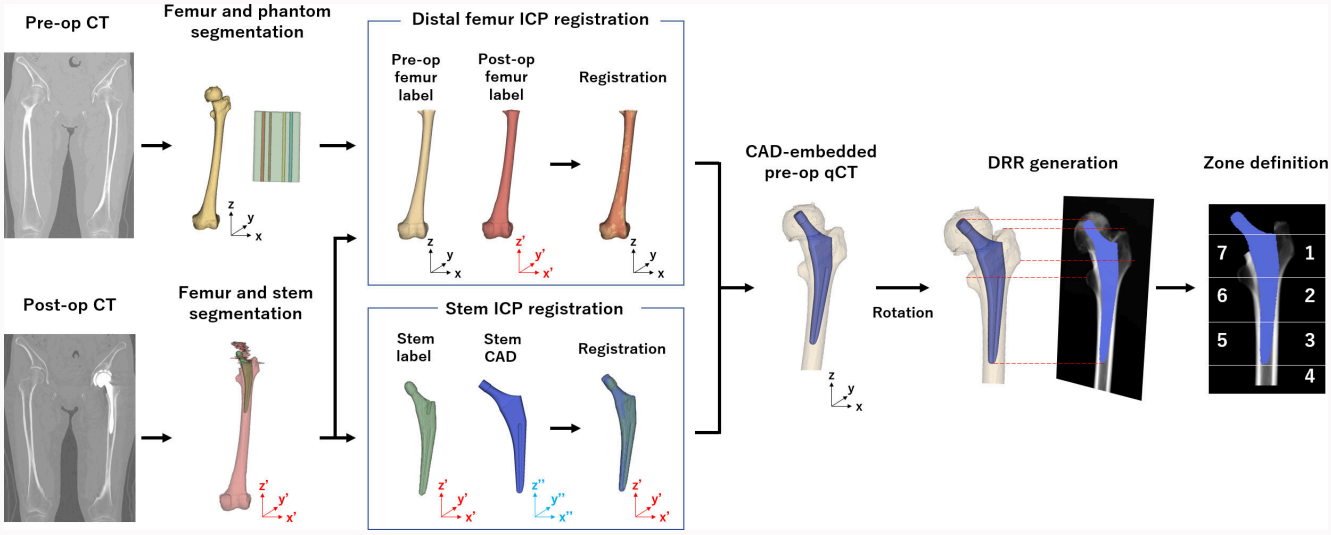

Fig. 1
Flowchart illustrating the process for measuring bone mineral density (BMD) at the Gruen zone (representative example of left femur). The femur and calibration phantom were segmented from preoperative (pre-op) CT images, and the femur and stem were segmented from postoperative (post-op) CT images. The segmented stem was registered to computer-aided design (CAD) models, and the preoperative and postoperative femur labels were also registered using an iterative closest point (ICP) registration. The CAD model was embedded in preoperative quantitative CT (CAD-embedded preop qCT) and was rotated to the neutral position and projected anteroposteriorly to generate a digitally reconstructed radiograph (DRR) to measure the BMD at Gruen zones 1 to 7. The coordinates indicated for each label indicate the preop CT coordinates (black), postop CT coordinates (red), and CAD coordinates (cyan).

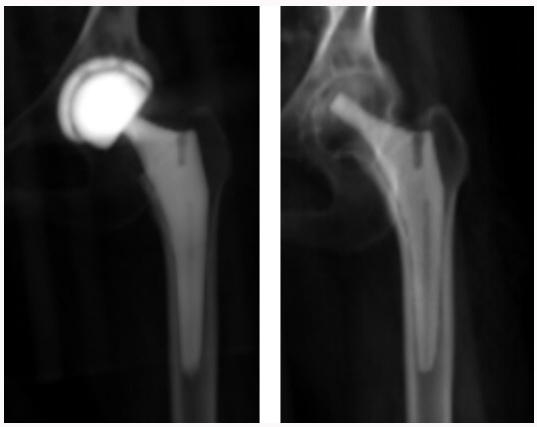

Fig. 2
Representative example of a digitally reconstructed radiograph (DRR) generated from a postoperative CT image (left) and a DRR generated from a computer-aided design-embedded preoperative CT image (right).

from postoperative CT images and the registered CAD model was calculated. Further, the surface distance between the femur models (distal to the lesser trochanter) segmented from preoperative and postoperative CT images after applying the registration was calculated. Finally, two orthopaedic surgeons (KU, SK) visually confirmed the DRR generated from postoperative CT images and those generated from the CAD-embedded preoperative qCT (Figure 2). In case of mismatch between the femoral neck cut line and the head-neck junction of the stem, the BMD analysis for zone 7 was not performed.

Rotation simulation

As the exact leg position during the acquisition of DXA images is unknown, the pose where the line connecting posterior condyles becomes parallel to the coronal plane was defined as neutral when performing the CT measurements. However, as this definition may not exhibit the patient positioning during DXA acquisition, an additional simulation altering the hip rotation was performed by changing the rotation of the femur. Specifically, the femur was rotated from −30° (external rotation) to +30° (internal rotation) with a 1° increment, and the BMD of the Gruen zone at each angle was measured and correlated to DXA-BMD of the identical zone (Figure 3). Simulations and measurements were performed computationally using MATLAB (v9.10; The MathWorks, USA).

Statistical analysis

The normality of continuous variables was assessed using the Shapiro-Wilk test. Normally distributed variables were expressed as mean (SD), whereas non-normally distributed variables were expressed as median (IQR). Correlations were assessed using the Spearman correlation coefficient (r_s) when data were non-normally distributed. Correlation coefficients of 0.60 to 0.79 were regarded as strong, and 0.80 to 1.00 as very strong.[34]

A priori power analysis was performed to determine the minimum required sample size for detecting a significant correlation between CT-aBMD and DXA-BMD measurements. Assuming an effect size of $r = 0.60$, two-sided $\alpha = 0.05$, and power of 80% and considering multiple comparisons across seven Gruen zones by applying the Bonferroni correction, the required sample size was 29. All statistical analyses were performed using MATLAB or G*Power software (version 3.1.9.6),[35] and p-values < 0.05 were considered indicative of statistical significance.

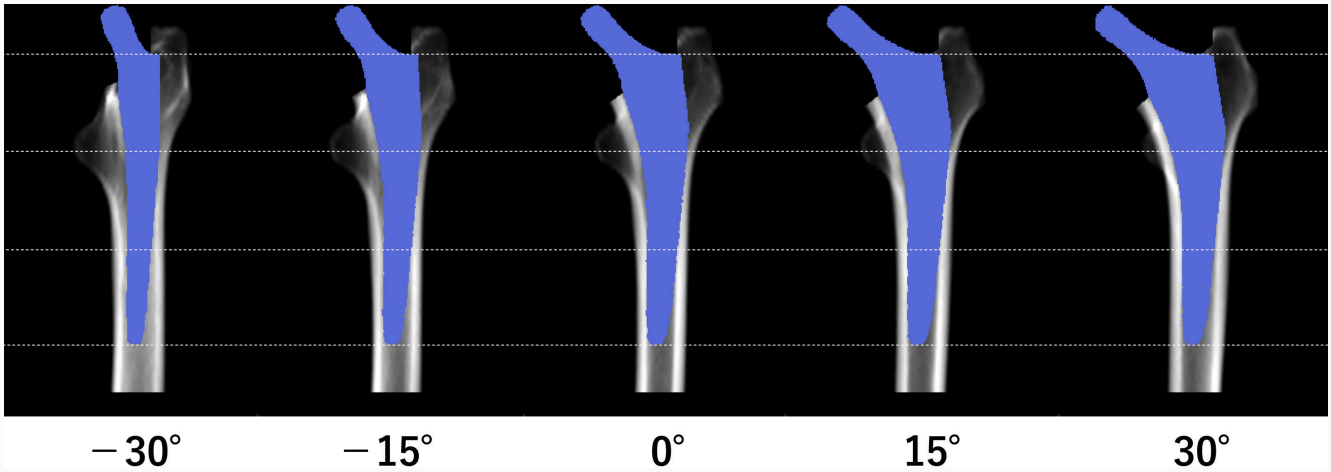

Fig. 3
Digitally reconstructed radiograph generated to measure bone mineral density at each Gruen zone shown here with 15° increments of rotation, while lines define the regions to determine the Gruen zones.

Table II. Results of the measurements by dual-energy x-ray absorptiometry (DXA) and quantitative CT (qCT) images.

Zones	BMC (DXA/qCT), g	Area (DXA/qCT), cm^2	BMD (DXA/qCT), g/cm^2
Zone 1	3.80 (3.27 to 4.53)/ 3.52 (2.82 to 4.18)	5.16 (4.51 to 5.76)/ 5.81 (5.08 to 6.34)	0.791 (0.665 to 0.871)/ 0.627 (0.542 to 0.723)
Zone 2	3.16 (2.33 to 3.99)/ 3.12 (2.31 to 3.82)	1.87 (1.54 to 2.29)/ 2.35 (2.01 to 2.75)	1.623 (1.516 to 1.801)/ 1.346 (1.175 to 1.459)
Zone 3	5.61 (4.75 to 6.28)/ 5.39 (4.79 to 5.91)	2.98 (2.57 to 3.39)/ 3.24 (3.04 to 3.78)	1.907 (1.731 to 2.084)/ 1.624 (1.487 to 1.747)
Zone 4	8.33 (7.32 to 9.49)/ 8.09 (7.28 to 9.39)	4.66 (4.43 to 4.92)/ 5.00 (4.75 to 5.37)	1.749 (1.609 to 1.982)/ 1.589 (1.472 to 1.820)
Zone 5	4.22 (3.39 to 5.14)/ 4.97 (3.97 to 5.93)	2.23 (1.88 to 2.57)/ 3.03 (2.48 to 3.39)	1.905 (1.732 to 2.025)/ 1.667 (1.529 to 1.821)
Zone 6	4.63 (3.82 to 5.31)/ 5.05 (4.39 to 5.84)	2.98 (2.59 to 3.47)/ 4.13 (3.66 to 4.74)	1.537 (1.387 to 1.707)/ 1.224 (1.072 to 1.370)
Zone 7	2.26 (1.77 to 2.87)/ 3.04 (2.61 to 3.61)	2.07 (1.55 to 2.42)/ 3.15 (2.78 to 3.61)	1.235 (1.015 to 1.335)/ 0.988 (0.875 to 1.117)

All values are expressed as median (IQR).
BMC, bone mineral content; BMD, bone mineral density.

Results

Two orthopaedic surgeons (KU, SK) visually confirmed that all the DRRs generated from postoperative CT images and those generated from the CAD-embedded preoperative qCT were well aligned. Three cases in which the neck cut line did not match the stem-neck junction were excluded from the analysis in zone 7. For the remaining hips, qCT measurements were automatically performed for all zones (Table II).

Comparison between CT and DXA measurements

When measurements of CT and DXA were compared, CT-BMC was larger or smaller than DXA-BMC, depending on the zones. However, CT-Area was significantly larger than DXA-Area, resulting in a smaller CT-aBMD than the DXA-BMD for all zones (Table II).

When correlated, the correlation between CT-BMC and DXA-BMC for each zone ranged between 0.782 and 0.967, with the strongest correlation observed in zone 4 and the weakest in zone 7 (Figure 4). For CT- and DXA-Areas, the correlation ranged between 0.724 and 0.864 with the strongest correlation in zone 6 and the weakest in zone 3 (Figure 5). For CT-aBMD and DXA-BMD, the correlation ranged between 0.677 and 0.924 with the strongest correlation in zone 1 and the weakest in zone 7 (Figure 6). All correlations were $p < 0.001$.

In the Bland-Altman analysis of comparing CT-aBMD and DXA-BMD for each zone, the ranges of LoA were 0.20, 0.49, 0.51, 0.37, 0.60, 0.46, and 0.60 g/cm^2 for zones 1 to 7, respectively (Figure 7).

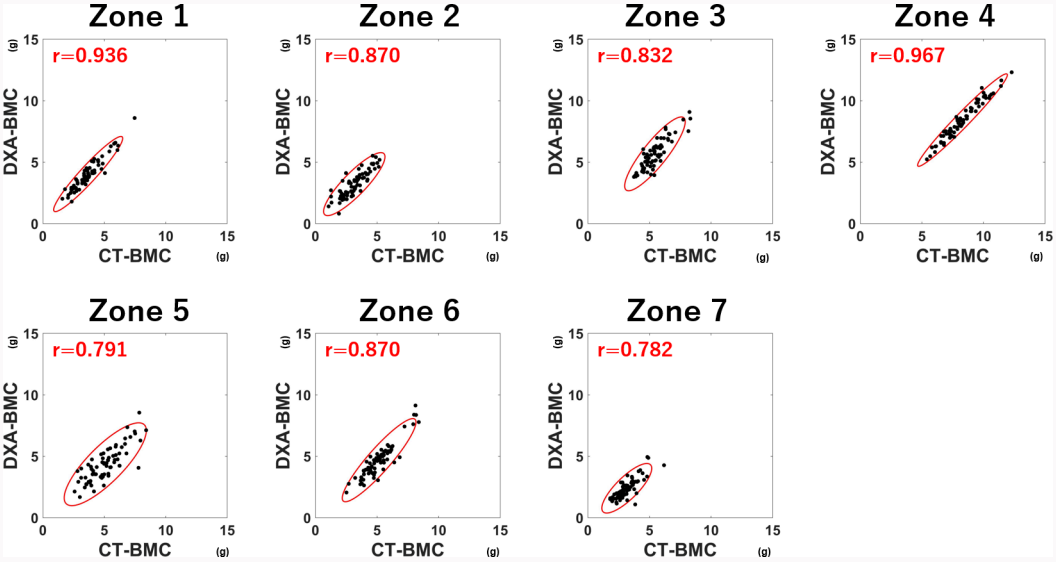

Fig. 4
Correlation between the bone mineral content measured from CT images (CT-BMC) and those measured from dual-energy x-ray absorptiometry (DXA-BMC) for Gruen zones 1 to 7. For each zone, a red ellipse illustrates the correlation structure between variables, where the shape and orientation of each ellipse reflect the strength and direction of the correlation; red letters denote the coefficient of determination.

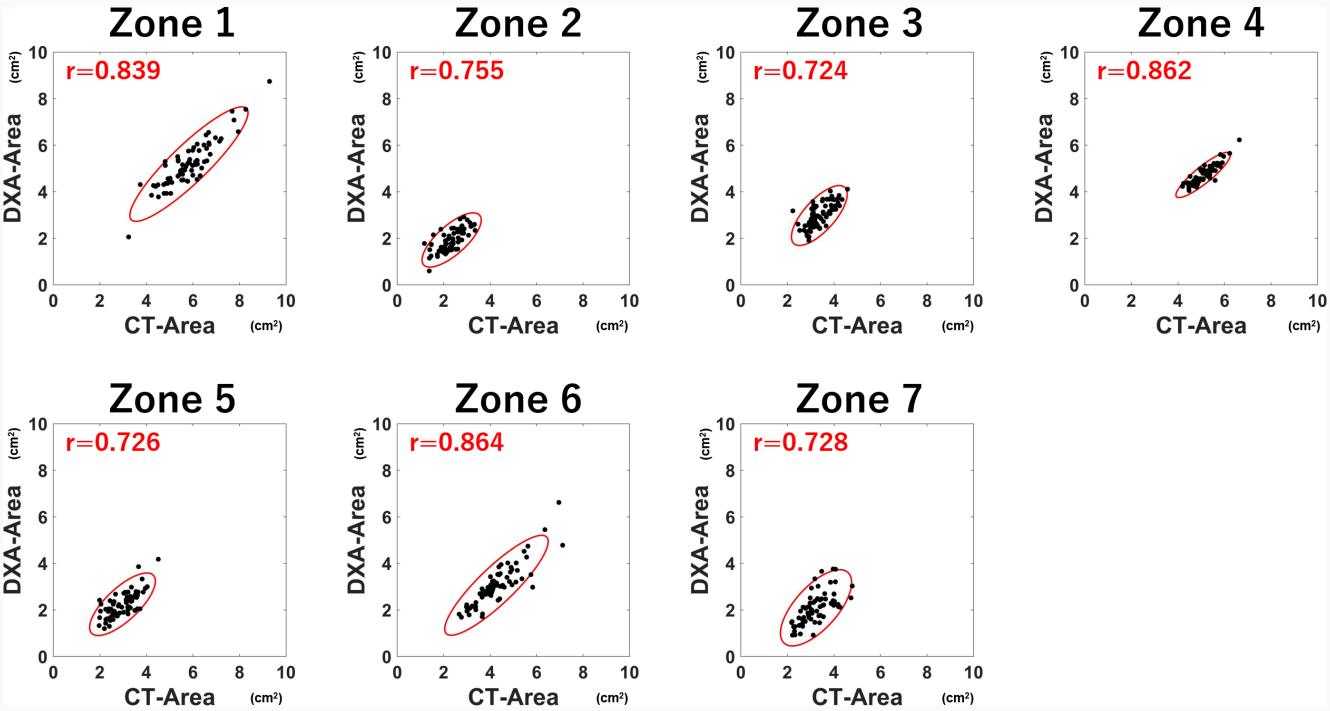

Fig. 5
Correlation between the area measured from CT images (CT-Area) and that measured from dual-energy x-ray absorptiometry (DXA-Area) for Gruen zones 1 to 7. For each zone, a red ellipse illustrates the correlation structure between variables, where the shape and orientation of each ellipse reflect the strength and direction of the correlation; red letters denote the coefficient of determination.

Validation

The median surface distance between the stem region segmented from postoperative CT images and the CAD model was 0.29 mm (IQR 0.26 to 0.33). The median surface distance between the femur models segmented from preoperative and postoperative CT images was 0.40 mm (IQR 0.38 to 0.43).

Effect of hip rotation

When the BMD at each Gruen zone was measured with the femur rotated from −30° (external rotation) to +30° (internal rotation) and was correlated to DXA-BMD, the strongest correlation ranged from 0.745 (zone 7) to 0.950 (zone 1) (Figure 8). The strongest correlation for zones 1 to 7 was observed with an internal rotation of 17°, 13°, 19°, 18°, 13°, 6°, and 19°, respectively (red circles in Figure 8).

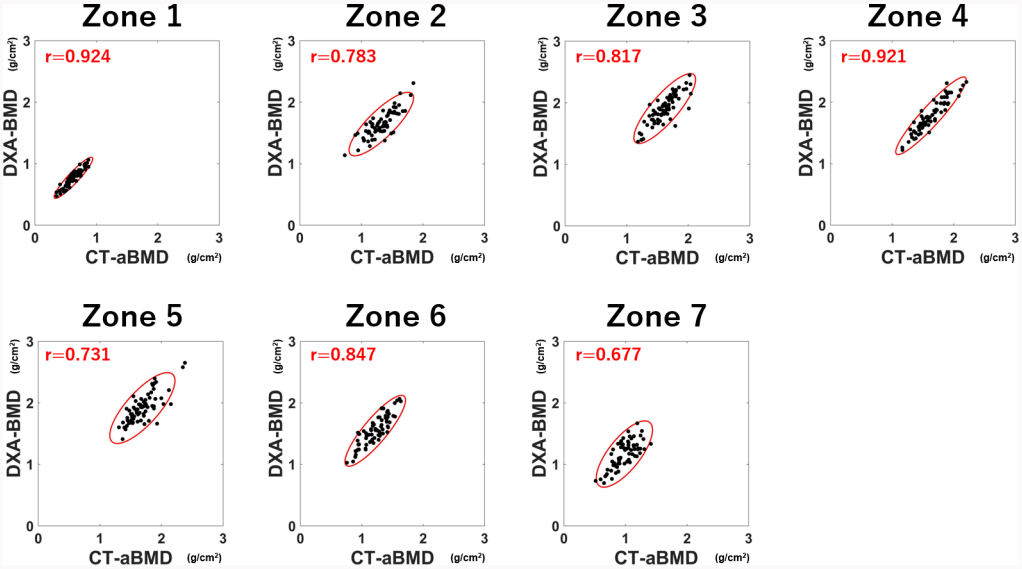

Fig. 6

Correlation between the bone mineral density measured from CT images (CT-aBMD) and that measured from dual-energy x-ray absorptiometry (DXA-BMD) for Gruen zones 1 to 7. For each zone, a red ellipse illustrates the correlation structure between variables, where the shape and orientation of each ellipse reflect the strength and direction of the correlation; red letters denote the coefficient of determination.

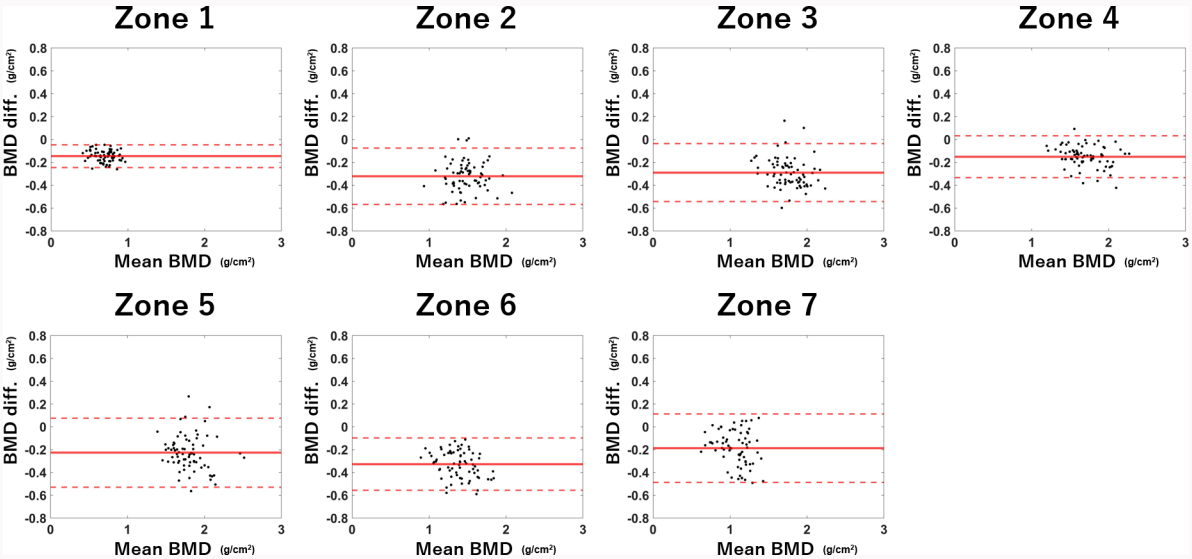

Fig. 7

Bland-Altman analysis of the bone mineral density measured from CT images (CT-aBMD) and dual x-ray absorptiometry BMD (DXA-BMD) for zones 1 to 7. For each zone, the red thick line indicates the mean value of the plots, and the thin red dotted lines indicate the 95% limits of agreement. BMD Diff., BMD difference (calculated by subtracting DXA-BMD from CT-aBMD).

Discussion

In this study, we used quantitative CT images to measure the BMD at the Gruen zones and compared the results with those measured from DXA. We found very strong correlations in zones 1, 3, 4, and 6, while the correlations in zones 2, 5, and 7 were also strong but relatively weaker (with coefficients < 0.8). In the simulation study altering hip rotation angles, the strongest correlation between CT-aBMD and DXA-BMD in zones 1 to 6 exceeded 0.78, while the maximum was limited to 0.745 for zone 7 (Figure 7). As BMD in zone 7 is predominantly important for taper-wedge type (e.g. Accolade II stem) for evaluating implant fixation and load transfer, our results suggest cautious measurement and evaluation of BMD in zone 7 using DXA.

In the BMC comparison, correlations exceeding 0.8 were observed between CT-BMC and DXA-BMC for all zones except for zones 5 and 7. For Area, correlations were lower than those for BMC with correlations below 0.8 in zones 2, 3, 5, and 7 ($p < 0.001$ for all). This was potentially attributable to errors in detecting the bone contour in the DXA software, which may be supported by CT-Area being larger than DXA-Area for all zones (Table II).

In the BMD comparison, very strong correlations ($r > 0.8$) were found between CT-aBMD and DXA-BMD for zones 1, 3, 4, and 6; however, the correlations in zones 2, 5, and 7 were

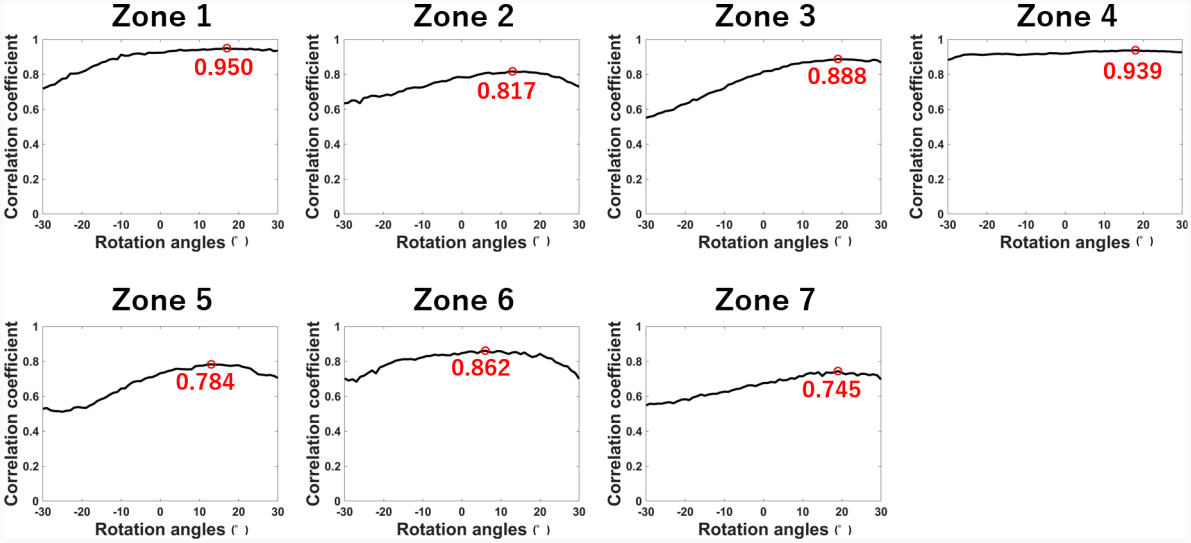

Fig. 8
Changes in the correlation coefficient between bone mineral density measured from CT images (CT-aBMD) and dual x-ray absorptiometry BMD (DXA-BMD) on altering the hip rotation angle from −30° (external rotation) to +30° (internal rotation) for Gruen zones 1 to 7. The red number and circle in each figure indicate the strongest correlation coefficient and the point where the strongest correlation was found.

weaker than 0.8 ($p < 0.001$ for all). Further, in the Bland-Altman analysis, the range of LoA was the largest in zones 5 and 7 (0.60 g/cm^2), indicating potential errors in measuring BMD by DXA in these zones. These results are consistent with previous studies that reported low precision during repeated measurements of the BMD at the Gruen zones for the same patients in a short interval.[18] For instance, an average precision of 6.7% has been reported for zone 7.[16]

On altering the hip rotation, changes in correlation coefficient were observed, which agrees with the results of previous studies reporting a large effect of hip positioning on the BMD measurement errors for the neck and total region of the hip.[9,36] Although the strongest correlations were > 0.8 for all zones, except for zones 5 and 7 (limited to 0.784 and 0.745, respectively), the results indicate that other factors may cause these measurement errors (e.g. ROI definition in DXA-Area).

The strongest correlations were observed when the femur was internally rotated for 6° to 19°. These results may be expected, as a previous study reported a mean angle of 10° between the patella and the posterior femoral condyle in patients undergoing THA,[37] supporting a slight internal rotation of the posterior condyles when the patella was set pointed forward during acquisition of DXA images.

Zones 1 and 7 are the main regions where the stem is coated by hydroxyapatite and rigid fixation of the stem to the femur is expected for taper-wedge stems. Therefore, many studies have focused on the longitudinal BMD changes at these zones. Although previous studies have reported the effects of stem insertion angle[19] and stem types on periprosthetic BMD,[13,14,20] our findings suggest the need to exercise caution during longitudinal BMD assessment using DXA, particularly in zone 7, as measurement errors could either obscure or exaggerate actual changes. We recommend that researchers at least check the precision error and evaluate the BMD changes by calculating the least significant change (LSC). Furthermore, we recommend carefully controlling the leg position during DXA acquisition and confirming the image on the DXA report when analyzing the BMD of the Gruen zones in longitudinal studies. For instance, the shape of the lesser trochanter and the ROI shown on the DXA report may be one of the references.

Some limitations of this study should be acknowledged. First, this study employed CT images and CAD models in which a novel method was applied. Thus, these approaches are yet to be widely used and may not be directly comparable with DXA. However, the median surface distance of the registration is smaller than the pixel size of the CT images, and the scripts used herein are available at https://github.com/keisuke-uemura/Gruen-zone-BMD so that researchers may reproduce our findings using these scripts. Moreover, as the qCT method to measure BMD of the proximal femur (i.e. regions without the stem) has been previously validated,[29] and a very strong correlation of 0.921 was observed in zone 4 in the present study (Figure 6), where the stem is not included, the analysis was likely performed in line with studies that have used qCT for measuring BMD, listed on the position paper of the ISCD.[24] Second, our findings are based on a single type of stem. Thus, our results may not be entirely generalizable to other types of stems. Although additional research is needed to investigate the applicability of the method to different stems, this study holds clinical importance given that it quantified the discrepancies in the measurement between DXA and qCT at the Gruen zones with a widely used cementless stem. Third, preoperative CT images and DXA acquired in the immediate phase after THA were used in this study (mean deviation: 5.5 weeks). Thus, the relationship between CT-aBMD and DXA-BMD may vary if the analysis were performed in a longitudinal study where stress shielding, including calcar rounding,[38] may occur. Although this could be a topic for future research, the analysis performed here remains clinically meaningful, as BMD measured in the early phase following THA usually stands as the reference for assessing BMD changes in longitudinal studies.

In summary, we measured the BMD in the Gruen zones using qCT and CAD models and assessed their correlation with DXA measurements. Although strong to very strong

correlations were observed in all zones, the correlation in zone 7, which plays an important role in stem fixation, was limited to 0.677. Based on the results, we recommend that doctors confirm if DXA was analyzed consistently, and carefully evaluate the BMD by assessing the precision error and calculating the LSC at their institution for each stem.

References

1. **Jain RK**, **Vokes T**. Dual-energy X-ray Absorptiometry. *J Clin Densitom*. 2017;20(3):291–303.
2. **Kanis JA**, **Cooper C**, **Rizzoli R**, **Reginster J-Y**, **Scientific Advisory Board of the European Society for Clinical and Economic Aspects of Osteoporosis (ESCEO) and the Committees of Scientific Advisors and National Societies of the International Osteoporosis Foundation (IOF)**. European guidance for the diagnosis and management of osteoporosis in postmenopausal women. *Osteoporos Int*. 2019;30(1):3–44.
3. **Uemura K**, **Miyamura S**, **Otake Y**, **et al**. The effect of forearm rotation on the bone mineral density measurements of the distal radius. *J Bone Miner Metab*. 2024;42(1):37–46.
4. **Cirnigliaro CM**, **Myslinski MJ**, **La Fountaine MF**, **Kirshblum SC**, **Forrest GF**, **Bauman WA**. Bone loss at the distal femur and proximal tibia in persons with spinal cord injury: imaging approaches, risk of fracture, and potential treatment options. *Osteoporos Int*. 2017;28(3):747–765.
5. **Oh JH**, **Song BW**, **Kim SH**, **et al**. The measurement of bone mineral density of bilateral proximal humeri using DXA in patients with unilateral rotator cuff tear. *Osteoporos Int*. 2014;25(11):2639–2648.
6. **Morgan SL**, **Prater GL**. Quality in dual-energy X-ray absorptiometry scans. *Bone*. 2017;104:13–28.
7. **Wong CP**, **Gani LU**, **Chong LR**. Dual-energy X-ray absorptiometry bone densitometry and pitfalls in the assessment of osteoporosis: a primer for the practicing clinician. *Arch Osteoporos*. 2020;15(1):135.
8. **Lekamwasam S**, **Lenora RSJ**. Effect of leg rotation on hip bone mineral density measurements. *J Clin Densitom*. 2003;6(4):331–336.
9. **Qutbi M**, **Salek A**, **Soltanshahi M**, **Ajdari SE**, **Asli IN**. The impact of nonstandard hip rotation on densitometric results of hip regions and potential misclassification of diagnosis. *Arch Osteoporos*. 2019;14(1):86.
10. **Uemura K**, **Takao M**, **Otake Y**, **et al**. The effect of patient positioning on measurements of bone mineral density of the proximal femur: a simulation study using computed tomographic images. *Arch Osteoporos*. 2023;18(1):35.
11. **Uemura K**, **Takao M**, **Otake Y**, **et al**. The effect of region of interest on measurement of bone mineral density of the proximal femur: simulation analysis using CT images. *Calcif Tissue Int*. 2022;111(5):475–484.
12. **Gruen TA**, **McNeice GM**, **Amstutz HC**. "Modes of failure" of cemented stem-type femoral components: a radiographic analysis of loosening. *Clin Orthop Relat Res*. 1979;141:17–27.
13. **Inaba Y**, **Kobayashi N**, **Oba M**, **Ike H**, **Kubota S**, **Saito T**. Difference in postoperative periprosthetic bone mineral density changes between 3 major designs of uncemented stems: a 3-year follow-up study. *J Arthroplasty*. 2016;31(8):1836–1841.
14. **Ohyama Y**, **Minoda Y**, **Masuda S**, **Sugama R**, **Ohta Y**, **Nakamura H**. Contact states with femoral cortical bone and periprosthetic bone mineral density changes differ between traditional and newly introduced fully hydroxyapatite-coated stems. *Bone Joint J*. 2024;106-B(6):548–554.
15. **Hooper G**, **Thompson D**, **Frampton C**, **et al**. Evaluation of proximal femoral bone mineral density in cementless total hip arthroplasty: a 3-arm prospective randomized controlled trial. *J Bone Joint Surg Am*. 2024;106-A(6):508–516.
16. **Nishii T**, **Sugano N**, **Masuhara K**, **Shibuya T**, **Ochi T**, **Tamura S**. Longitudinal evaluation of time related bone remodeling after cementless total hip arthroplasty. *Clin Orthop Relat Res*. 1997;339:121–131.
17. **Kröger H**, **Miettinen H**, **Arnala I**, **Koski E**, **Rushton N**, **Suomalainen O**. Evaluation of periprosthetic bone using dual-energy x-ray absorptiometry: precision of the method and effect of operation on bone mineral density. *J Bone Miner Res*. 1996;11(10):1526–1530.
18. **Kröger H**, **Venesmaa P**, **Jurvelin J**, **Miettinen H**, **Suomalainen O**, **Alhava E**. Bone density at the proximal femur after total hip arthroplasty. *Clin Orthop Relat Res*. 1998;352:66–74.
19. **Maeda T**, **Kuroda Y**, **Kamenaga T**, **Matsumoto T**, **Kuroda R**, **Hayashi S**. Impact of femoral stem alignment on periprosthetic bone density in THA: a study of the Avenir complete stem. *Arch Orthop Trauma Surg*. 2024;145(1):74.
20. **Rilby K**, **Mohaddes M**, **Kärrholm J**. Similar results after five years with the use of the Fitmore or the CLS femoral components. *Bone Jt Open*. 2023;4(5):306–314.
21. **Morita A**, **Iida Y**, **Inaba Y**, **et al**. Preoperative prediction for periprosthetic bone loss and individual evaluation of bisphosphonate effect after total hip arthroplasty using artificial intelligence. *Bone Joint Res*. 2024;13(4):184–192.
22. **Martini F**, **Lebherz C**, **Mayer F**, **Leichtle U**, **Kremling E**, **Sell S**. Precision of the measurements of periprosthetic bone mineral density in hips with a custom-made femoral stem. *J Bone Joint Surg Br*. 2000;82-B(7):1065–1071.
23. **Mortimer ES**, **Rosenthall L**, **Paterson I**, **Bobyn JD**. Effect of rotation on periprosthetic bone mineral measurements in a hip phantom. *Clin Orthop Relat Res*. 1996;324(324):269–274.
24. **Engelke K**, **Lang T**, **Khosla S**, **et al**. Clinical use of quantitative computed tomography (QCT) of the hip in the management of osteoporosis in adults: the 2015 ISCD official positions-Part I. *J Clin Densitom*. 2015;18(3):338–358.
25. **World Medical Association**. World Medical Association Declaration of Helsinki: ethical principles for medical research involving human subjects. *JAMA*. 2013;310(20):2191–2194.
26. **American Academy of Orthopaedic Surgeons (AAOS)**. American Joint Replacement Registry (AJRR): 2024 Annual Report, 2024. https://www.aaos.org/registries/publications/ajrr-annual-report/ (date last accessed 18 September 2025).
27. **Australian Orthopaedic Association National Joint Replacement Registry (AOANJRR)**. Hip, Knee & Shoulder Arthroplasty Annual Report, 2020. https://aoanjrr.sahmri.com/annual-reports-2020 (date last accessed 18 September 2025).
28. **Kuribayashi M**, **Takahashi KA**, **Fujioka M**, **Ueshima K**, **Inoue S**, **Kubo T**. Reliability and validity of the Japanese Orthopaedic Association hip score. *J Orthop Sci*. 2010;15(4):452–458.
29. **Uemura K**, **Otake Y**, **Takashima K**, **et al**. Development and validation of an open-source tool for opportunistic screening of osteoporosis from hip CT images. *Bone Joint Res*. 2023;12(9):590–597.
30. **Sakamoto M**, **Hiasa Y**, **Otake Y**, **et al**. Bayesian segmentation of hip and thigh muscles in metal artifact-contaminated CT using convolutional neural network-enhanced normalized metal artifact reduction. *J Sign Process Syst*. 2020;92(3):335–344.
31. **Hiasa Y**, **Otake Y**, **Takao M**, **Ogawa T**, **Sugano N**, **Sato Y**. Automated muscle segmentation from clinical CT Using Bayesian U-Net for personalized musculoskeletal modeling. *IEEE Trans Med Imaging*. 2020;39(4):1030–1040.
32. **Besl PJ**, **McKay ND**. A method for registration of 3-D shapes. *IEEE Trans Pattern Anal Mach Intell*. 1992;14(2):239–256.
33. **Uemura K**, **Otake Y**, **Takao M**, **et al**. Automated segmentation of an intensity calibration phantom in clinical CT images using a convolutional neural network. *Int J Comput Assist Radiol Surg*. 2021;16(11):1855–1864.
34. **Landis JR**, **Koch GG**. The measurement of observer agreement for categorical data. *Biometrics*. 1977;33(1):159.
35. **Faul F**, **Erdfelder E**, **Lang AG**, **Buchner A**. G*Power 3: a flexible statistical power analysis program for the social, behavioral, and biomedical sciences. *Behav Res Methods*. 2007;39(2):175–191.
36. **Rosenthall L**. Range of change of measured BMD in the femoral neck and total hip with rotation in women. *J Bone Miner Metab*. 2004;22(5):496–499.
37. **Akiyama K**, **Nakata K**, **Kitada M**, **et al**. Changes in axial alignment of the ipsilateral hip and knee after total hip arthroplasty. *Bone Joint J*. 2016;98-B(3):349–358.
38. **Engh CA**, **Bobyn JD**. The influence of stem size and extent of porous coating on femoral bone resorption after primary cementless hip arthroplasty. *Clin Orthop Relat Res*. 1988;231:7–28.

Author information

K. Uemura, MD, PhD, Associate Professor
N. Sugano, MD, PhD, Professor
H. Hamada, MD, PhD, Associate Professor
Department of Orthopaedic Medical Engineering, Osaka University Graduate School of Medicine, Suita, Japan.

Y. Otake, PhD, Associate Professor, Division of Information Science, Graduate School of Science and Technology, Nara Institute of Science and Technology, Ikoma, Japan.

K. Tamura, MD, PhD, Orthopaedic Surgeon, Department of Orthopaedics, Kyowakai Hospital, Suita, Japan.

R. Higuchi, MD, Doctoral Student
S. Kono, MD, Doctoral Student
H. Mae, MD, PhD, Assistant Professor
K. Takashima, MD, PhD, Assistant Professor
S. Okada, MD, PhD, Professor
Department of Orthopaedic Surgery, Osaka University Graduate School of Medicine, Suita, Japan.

Author contributions

K. Uemura: Conceptualization, Formal analysis, Funding acquisition, Investigation, Methodology, Project administration, Software, Visualization, Writing – original draft.
Y. Otake: Funding acquisition, Methodology, Resources, Software, Writing – review & editing.
K. Tamura: Resources, Writing – review & editing.
R. Higuchi: Writing – review & editing.
S. Kono: Writing – review & editing.
H. Mae: Writing – review & editing.
K. Takashima: Writing – review & editing.
S. Okada: Supervision.
N. Sugano: Resources, Supervision, Writing – review & editing.
H. Hamada: Resources, Writing – review & editing.

Funding statement

The authors disclose receipt of the following financial or material support for the research, authorship, and/or publication of this article: Grant-in-Aid for Science Research from the Japanese Society for Replacement Arthroplasty Foundation (2023-RP05), and Japan Society for the Promotion of Science Grants-in-Aid for Scientific Research (KAKENHI; grant numbers 20H04550, 21K16655, and 24K19617), as well as the CAD model from Stryker.

ICMJE COI statement

K. Uemura and Y. Otake report grant support from the Japan Society for the Promotion of Science (JSPS) Grants-in-Aid for Scientific Research (KAKENHI). K. Uemura also reports grant support from The Japanese Society for Replacement Arthroplasty Foundation, and the CAD model from Stryker.

Data sharing

The datasets generated and analyzed in the current study are not publicly available due to data protection regulations. Access to data is limited to the researchers who have obtained permission for data processing. The scripts used for analysis can be found at https://github.com/keisuke-uemura/Gruen-zone-BMD. Further inquiries can be made to the corresponding author.

Acknowledgements

We thank Dr. Nobuo Nakamura, Mr. Yasushi Shimoo and Mr. Tomoki Shimamura for their help in data acquisition, Drs. Yoshinobu Sato and Masaki Takao for their insightful comments, and Mr. Kazuki Suehara for his help in the analysis. We also thank Stryker (USA) for providing the CAD models of the stem implant.

Open access funding

The authors report that the open access funding for this manuscript was self-funded.